

Supplementary Materials for “Deep near-light photometric stereo for spatially varying reflectances”

Hiroaki Santo, Michael Waechter, and Yasuyuki Matsushita

Graduate School of Information Science and Technology,
Osaka University, Osaka, Japan
{santo.hiroaki, waechter.michael, yasumat}@ist.osaka-u.ac.jp

In this supplementary material,

- A. we give additional details about our synthetic dataset,
- B. we evaluate the performance of the proposed surface normal and reflectance estimation network (extended PS-FCN) on a distant-light photometric stereo dataset [3],
- C. we show the results of reflectance estimation on our synthetic dataset,
- D. we discuss the effect of perspective projection.

A Synthetic dataset

For our synthetic dataset in the main paper, to render the scenes with general BRDFs, we randomly selected some materials from the MERL BRDF database [2] for each scene. For *Bunny* and *Ganesha* we used the following five materials:

Bunny: BLUE-METALLIC-PAINT, FRUITWOOD-241, GREEN-METALLIC-PAINT, IPSWICH-PINE-221, and SPECIAL-WALNUT-224

Ganesha: CHERRY-235, GOLD-METALLIC-PAINT, GREEN-LATEX, NATURAL-209, and PICKLED-OAK-260

For *Blob03* we used Lambertian reflectance.

B Validation of extended PS-FCN

In Sec. 4.2 of the paper, we introduced an extension of PS-FCN [1] for joint estimation of surface normals *and* reflectances. The differences in terms of surface normal estimation are (1) normalization of the inputs and (2) simultaneous

Table S1. Comparison of the original PS-FCN [1] vs. our extended PS-FCN on the DiLiGenT datasets. Values are mean angular errors in degrees. The better results for each scene are marked up by bold font.

	ball	bear	buddha	cat	cow	goblet	harvest	pot1	pot2	reading	avg.
Original PS-FCN	2.8	7.6	7.9	6.2	7.3	8.6	15.9	7.1	7.3	13.3	8.4
Extended PS-FCN	2.9	7.4	9.0	4.6	8.0	8.1	14.6	5.6	8.7	12.9	8.2

training of the surface normal and reflectance estimator networks. To verify that these changes did not degrade the accuracy of the surface normal estimation, we compared the original with the extended PS-FCN on the DiLiGenT dataset [3], which is a distant light dataset. Table S1 shows the mean angular errors for the original and the extended PS-FCN. We can see that the accuracies are on average very similar.

Since the extended PS-FCN estimates reflectances in addition to normals, we also show results of reflectance estimation for the DiLiGenT dataset. Figures S1 and S2 show re-renderings of DiLiGenT scenes using the estimated reflectances. We can see that the obtained reflectance estimates are quite good in most scenes.

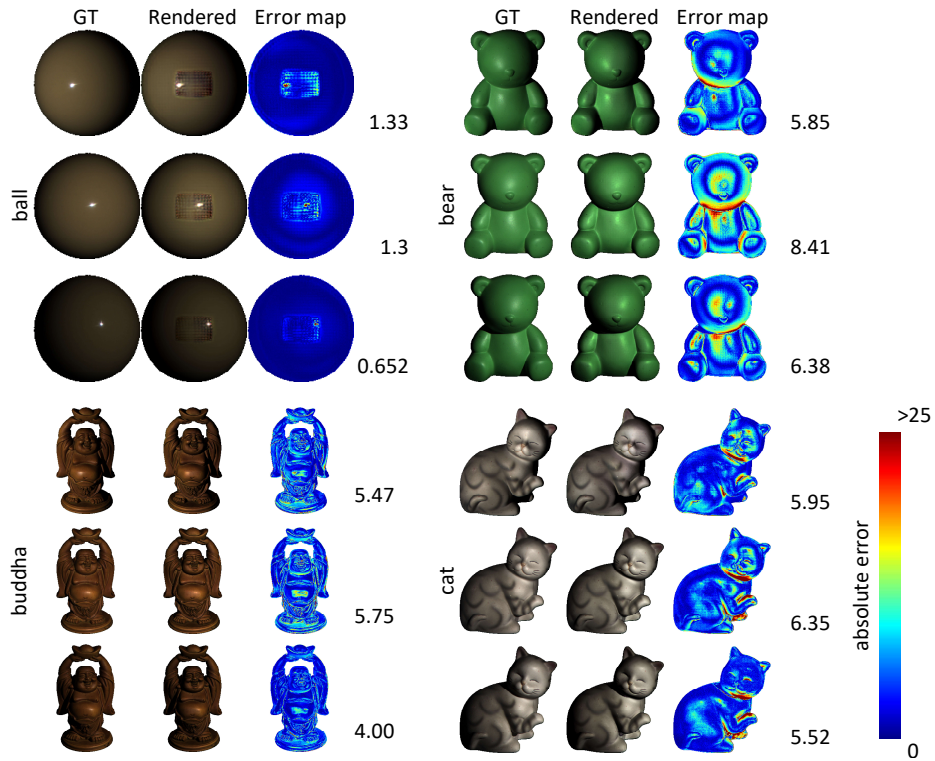


Fig. S1. Part 1 of our re-rendering results of extended PS-FCN on DiLiGenT. For each scene, we selected 3 light conditions out of the 96 available ones. “GT” are the ground truth observations (*i.e.*, input images) and “Rendered” are rendered images using the estimated reflectances. The error maps visualize the absolute error and the numbers next to the error maps are the mean absolute errors in a scaled intensity from 0 to 255. For better visualization, we applied brightness correction to the *ball*, specifically a scaling of intensities by the same factor for both the ground truth and the rendered images.

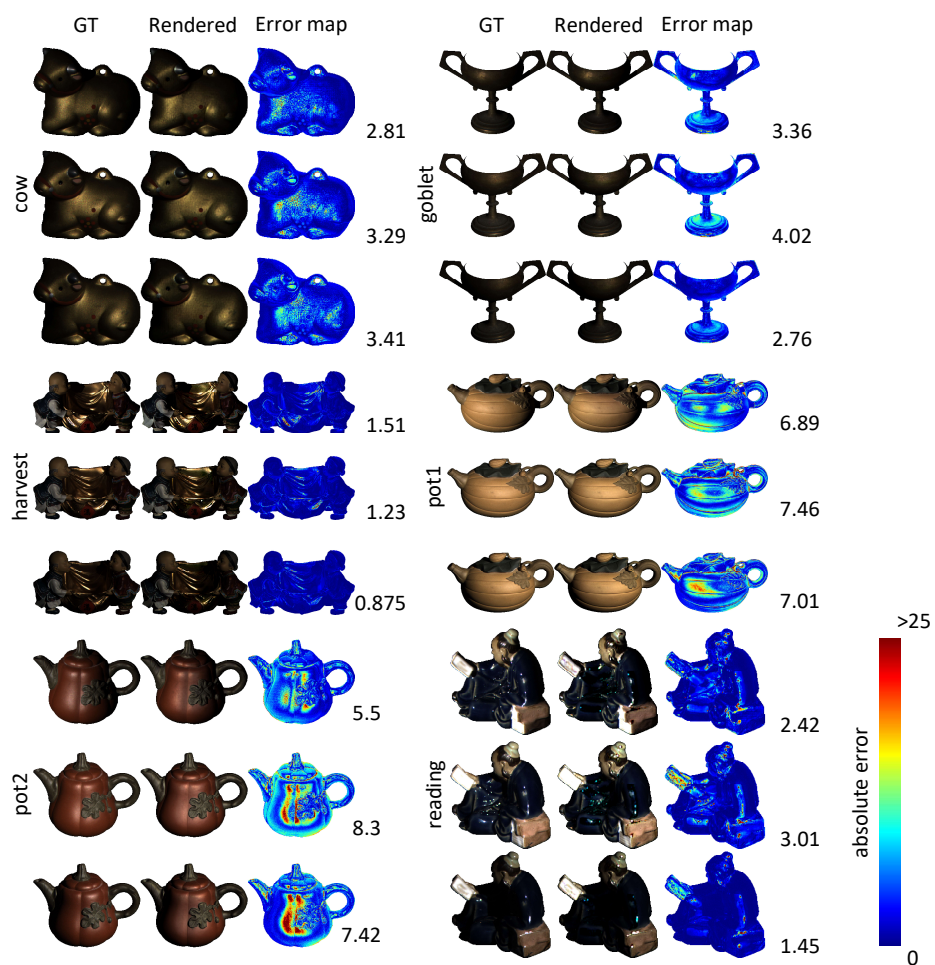


Fig. S2. Part 2 of our re-rendering results of extended PS-FCN on DiLiGenT. For better visualization, we applied brightness correction to *harvest* and *reading*.

C Validation of reflectance estimation

In Sec. 5 of the main paper, we only showed results of reflectance estimation on our real-world dataset. Figure S3 shows re-renderings for our synthetic dataset using estimated reflectances. We can see that the obtained reflectance estimates are quite good in most scenes.

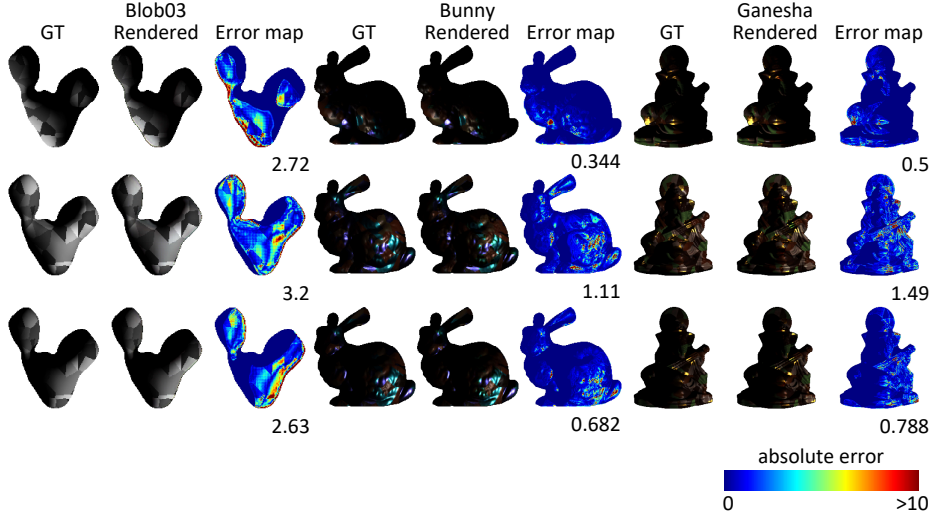


Fig. S3. Re-rendering results of our method for our synthetic dataset. For each scene, we selected 3 light conditions out of the 100 available ones. Each row corresponds to one lighting condition. “GT” and “Rendered” are the ground truth observations (*i.e.*, input images) and rendered images using the estimated reflectances, respectively. The error maps visualize the absolute error and the numbers underneath the error maps are the mean absolute errors in a scaled intensity from 0 to 255. For better visualization, we applied brightness correction to the *Bunny* and *Ganesha*, specifically a scaling of intensities by the same factor for both the ground truth and the rendered images.

D Effect of perspective projection

As discussed in Sec. 6 of the main paper, here we demonstrate the effect of differences in focal length on the proposed surface normal estimation network. We created synthetic scenes of *Blob03* with uniform Lambertian reflectance and varying focal length. To keep the scene size, we changed the camera position according to the focal length. All other settings were identical to the experiments in Sec. 5.1. We used the ground truth of the scene shape \mathbf{p}_i to calculate the pseudo observation \mathbf{m}'_{ij} in Eq. (4) and per-pixel lighting direction \mathbf{l}_{ij} in Eq. (1) and fed them to the surface normal estimation network $\text{PS}(\cdot)$ of Eq. (6) to obtain a prediction of the normal map.

With focal lengths of 120, 60, 30, 15, and 7.5 mm (35 mm-equivalent), the mean angular errors were 1.89° , 1.92° , 1.95° , 2.01° , and 2.08° , respectively. We can see that shorter focal lengths produce larger perspective distortion and therefore increase the estimation error, but not in a very significant way.

References

1. Chen, G., Han, K., Wong, K.Y.K.: PS-FCN: A flexible learning framework for photometric stereo. In: European Conference on Computer Vision (ECCV) (2018) [1](#)
2. Matusik, W., Pfister, H., Brand, M., McMillan, L.: A data-driven reflectance model. Transactions on Graphics (TOG) **22**(3), 759–769 (Jul 2003) [1](#)
3. Shi, B., Mo, Z., Wu, Z., Duan, D., Yeung, S.K., Tan, P.: A benchmark dataset and evaluation for non-Lambertian and uncalibrated photometric stereo. Transactions on Pattern Analysis and Machine Intelligence (PAMI) **41**(2), 271–284 (2019) [1](#), [2](#)